metals

MDPI

Review

The κ-Carbides in Low-Density Fe-Mn-Al-C Steels: A Review on Their Structure, Precipitation and Deformation Mechanism

Peng Chen [1,2,*], Xiaowu Li [1,2,3] and Hongliang Yi [2,*]

[1] Department of Materials Physics and Chemistry, School of Materials Science and Engineering, Northeastern University, Shenyang 110819, China; xwli@mail.neu.edu.cn
[2] The State Key Laboratory of Rolling and Automation, Northeastern University, Shenyang 110819, China
[3] Key Laboratory for Anisotropy and Texture of Materials, Northeastern University, Shenyang 110819, China
* Correspondence: chenpeng@mail.neu.edu.cn (P.C.); hityihl@126.com (H.Y.)

Received: 3 July 2020; Accepted: 27 July 2020; Published: 29 July 2020

Abstract: Fe-Mn-Al-C steels exhibit an outstanding combination of strength and ductility, and the addition of aluminum drastically reduces the density of steels. The low density also offers the advantage of lightweight structures compared with other alloys in practical applications. The addition of aluminum leads to an increased probability of κ-carbide precipitation, which would significantly affect the mechanical properties. This paper aims to review the κ-carbide in Fe-Mn-Al-C steels, including the structure, elastic and magnetic properties of κ-carbide, the precipitation mechanism of κ-carbide involving thermodynamic equilibrium, and the operative deformation mechanism of κ-carbide that governs the mechanical properties. It is hoped that such a comprehensive summarization of the knowledge of κ-carbide will be beneficial for the further development of low-density Fe-Mn-Al-C steels.

Keywords: κ-carbide; low-density steels; structure; precipitation; deformation mechanism

1. Introduction

Fe-Mn-Al-C steels were developed as a substitute for Fe-Cr-Ni stainless steels in the 1950s [1]. Recently, high-performance Fe-Mn-Al-C low-density steels have become attractive for potential applications in the production of structural parts, especially in the automotive industry, as they are able to simultaneously satisfy the requirements of reducing energy consumption while improving safety standards [2–5]. Fe-Al-Mn-C steels possess outstanding mechanical properties, with a yield strength of 0.4–1.0 GPa, an ultimate tensile strength of 0.6–2.0 GPa, and an elongation of 30–100% [3,5–9]. With respect to the range of chemical compositions, they can be an austenite matrix, a ferrite matrix, or duplex (ferrite and austenite) [10,11]. Manganese and carbon act as austenite stabilizers, while aluminum is a ferrite stabilizer. In addition, a specific weight reduction can be achieved in these steels through the addition of aluminum, since the aluminum element has a low atomic mass and causes a lattice expansion [12]. There will be a 1.3% density reduction per 1 wt.% addition of aluminum [3].

The addition of aluminum also accelerates the precipitation of ordered perovskite structure carbide, i.e., κ-carbide [9,13–15]. In the initial stages of the study of κ-carbide, it was thought to be harmful to ductility, and boron, titanium and niobium were normally added to suppress the precipitation of κ-carbide [16–18]. It has more recently been recognized that κ-carbide can simultaneously enhance strength and ductility by optimizing its fraction, morphology, size and distribution [19,20]. The intergranular κ-carbide is usually undesirable, while the intragranular nano-sized κ-carbide is popular for the improvement of mechanical properties [19].

In this review paper, the structure and precipitation mechanism of κ-carbide, as well as its influence on the mechanical properties of low-density Fe-Mn-Al-C steels, are summarized. Studies on κ-carbide in Fe-Mn-Al-C steels are reported in some cases. However, a deeper understanding of the intrinsic properties and equilibrium thermodynamics are required in order to make better use of κ-carbide. The deformation mechanism of Fe-Mn-Al-C steels related to κ-carbide is complicated. An appropriate assessment of the effective mechanism of κ-carbide on the microstructure evolution and mechanical behavior is needed for the further development of Fe-Mn-Al-C steels.

2. General Properties

2.1. Structural Properties

In the Fe-Al-C system, the κ-carbide is a ternary carbide with an $E2_1$ structure (Strukturbericht Designation), otherwise known as a perovskite structure [13–15,21]. This structure is based on the face-centered cubic (fcc) ordered Fe_3Al-$L1_2$ structure, with iron atoms located at the center of each face, aluminum atoms sitting on the corners of the cube and carbon atom occupying the central octahedral interstitial position formed by the six iron atoms as the first nearest neighbors (space group $Pm\bar{3}m$) (Figure 1) [14,22]. The perfect arrangement of this type corresponds to the formula of Fe_3AlC, while this stequiometry has not been experimentally observed [21,23]. As experimentally reported by Andryushchenko et al. [24], the stequiometry of κ-carbide was proposed to be $Fe_{4-y}Al_yC_x$ with $0.8 < y < 1.2$ and $0 < x < 1$. Some other studies have indicated that the stequiometry of κ-carbide is probably close to $Fe_3AlC_{x=0.5}$ [23,25], and that the formula is described as being Fe_3AlC_x, where x varies from 0.5 to 1 [26,27]. The lattice parameter of κ-carbide in the Fe-Al-C system changes with the composition, and it has been calculated and measured in many investigations (Table 1). It has been reported that the dependence of the lattice parameters on carbon concentration can be described in the following form: $a_{\kappa\text{-carbide}} = 3.7605 + 0.0295$ at.%C [14]. With the introduction of manganese into the Fe-Al-Mn-C system, the manganese atom occupies the same position as iron in the κ-carbide lattice, and it has a continues spectrum when varying the manganese content from Fe_3AlC to Mn_3AlC, which is expressed as $(Fe,Mn)_3AlC$ [2,28]. The lattice parameter a_0 increases as the manganese content rises, due to manganese having a larger atom radius (132 pm) than that of iron (127 pm).

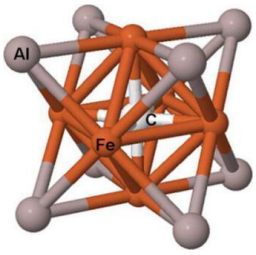

Figure 1. Conventional cell of κ-Fe_3AlC carbide. Please note that white balls represent carbon atoms, grey balls represent aluminum atoms, and orange balls represent iron atoms. (Reprinted with permission from [21], copyright Elsevier, 2008).

Table 1. The lattice parameters of κ-carbide given by relevant references.

κ-Carbide	a0 (Å)	Reference
Fe3AlC	3.75 (sp)	[21]
	3.73 (np)	
	3.78	[23]
	3.72–3.78	[26,27]
	3.783–3.79	[14]
	3.76	[22]
Fe2MnAlC	3.78	[22]
FeMn2AlC	3.80	[22]
Mn3AlC	3.81	[22]
	3.875	[29]

sp—spin polarized, and np—without spin effects.

2.2. Elastic and Magnetic Properties

It is well known that κ-Fe_3AlC carbide is formed by the insertion of a carbon atom at the octahedral site surrounded by six iron atoms of Fe_3Al-Ll_2. The insertion of carbon significantly influences the elastic constants [21], and softens the magnetic properties [30]. The elastic constants and bulk modulus (B_0) calculated by previous investigators are listed in Table 2. For the cubic system of Fe_3AlC and Mn_3AlC, there are only three independent elastic constants—C_{11}, C_{12} and C_{44}—while the tetragonal structure of Fe_2MnAlC and $FeMn_2AlC$ have an additional three independent elastic constants—C_{13}, C_{33}, and C_{66}. A comparison of Fe_3Al-Ll_2 and Fe_3AlC indicates that Fe_3AlC is stiffer and more anisotropic, and carbon rigidifies the crystal. The elastic constants and bulk modulus of Mn_3AlC are higher than those of Fe_3AlC, due to the Mn-C bond being stronger than the Fe-C bond. The fact that C_{33} for Fe_2MnAlC and C_{11} for $FeMn_2AlC$ are higher than C_{11} for Fe_2MnAlC and C_{33} for $FeMn_2AlC$ is also a result of the stronger Mn-C bond. Briggs et al. [31] also reported that manganese has a greater affinity with carbon. As a consequence, the introduction of carbon and manganese makes the crystal harder [32].

Table 2. The elastic constants and bulk modulus of Fe_3Al-Ll_2 and κ-carbides (in GPa).

Material	C11	C12	C44	C13	C33	C66	B0	Reference
Fe3Al-Ll2	185	160	124	-	-	-	168	[32]
	184	145	160	-	-	-	158	[21]
Fe3AlC	426	91	65	-	-	-	203	[32]
	453	100	69	-	-	-	215	[21]
Fe2MnAlC	422	74	92	92	463	92	202	[32]
FeMn2AlC	465	86	96	138	455	100	234	
Mn3AlC	454	100	106	-	-	-	218	

It has been stated that κ-carbide is ferromagnetic, with a Curie temperature between 125 °C and 290 °C [21,33], while some investigations have shown that κ-carbide might not be magnetic [24,34]. This is due to the strong interactions of Fe-C and Fe-Al, which may result in the quenching of the magnetic moment, therefore resulting in κ-carbide being non-magnetic [35]. The insertion of carbon significantly decreases the magnetic properties, with reduction of more than 50% [30]. A study by Reddy and Deevi [36] found that the local interactions of carbon in Fe_3AlC govern the magnetic properties that contribute to the atomic arrangement. In contrast to carbon, manganese substitution enhances

the magnetic properties of κ-carbide, except for Fe_2MnAlC [32]. The enhancement of magnetism is caused by the fact that the local magnetic moment of manganese is larger than that of iron, and the abnormal response of Fe_2MnAlC is a result of the reduction of the Fe moment overcompensating for the enhancement of the local moment upon Mn substitution [32].

3. Precipitation Mechanism

3.1. Equilibrium Thermodynamics

The Fe-Mn-Al-C steels have received a great deal of attention, which has been driven by the requirements of industry. Fe-Mn-Al-C steels exhibit a high density reduction, a high corrosion resistance, and a high strength–ductility match [3,5–9]. κ-carbide precipitation has an important effect on the mechanical and other properties of Fe-Mn-Al-C steels. For the detailed control of properties, it is essential to understand the microstructural constitution and evolution. Therefore, many investigations have recently calculated and measured equilibrium diagrams of Fe-Mn-Al-C steels involving the κ-carbide [9,13,23,37–42]. The Fe-C-Al system was first established covering a wide temperature range by Kumar and Raghavan [43], and some updates have subsequently been achieved [44–46], which is quite helpful for us to understand the formation of κ-carbide. The isothermal sections of the Fe-C-Al ternary system were calculated, and the Gibbs energies of κ-carbide formation were obtained [43]. Palm et al. [23] measured the phase equilibrium using an experimental method, and the properties of κ-carbide were also determined. Based on the thermodynamic description of the Fe-Al-C system and an existing database of Fe-based alloys, Chin et al. constructed the Fe-Mn-Al-C quaternary system (Figure 2), which exhibited a better fit with the experimental results when evaluating the stability of κ-carbide [13]. Considering the properties of liquids and optimizing the model parameters of κ-carbide, Kim et al. [39,42] and Phan et al. [47] developed a more accurate thermodynamic database, which could be used in the design of Fe-Mn-Al-C steels by predicting their phase evolution during heat treatment and κ-carbide precipitation.

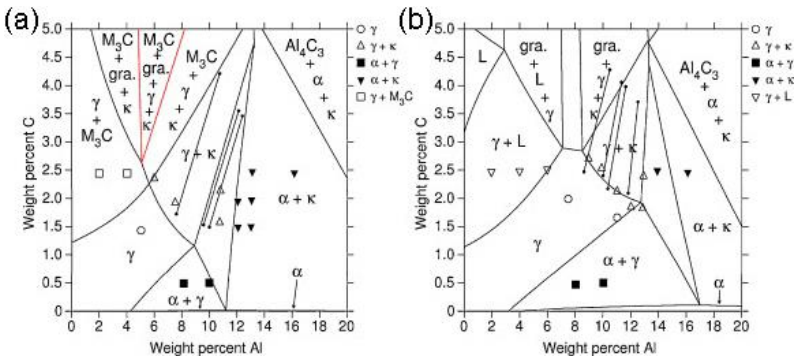

Figure 2. Calculated phase relations of Fe-20Mn-Al-C alloys at 900 °C (**a**) and 1200 °C (**b**), in comparison with experimental results. (Reprinted with permission from [13], copyright Elsevier, 2010).

3.2. Formation of κ-Carbide in Austenite Matrix

The observation of κ-carbide in austenite (Figure 3) indicates a typical microstructure by spinodal decomposition, which is mainly determined by the composition fluctuation of aluminum and carbon, and there is no nucleation stage [15,48]. Actually, the spinodal decomposition mechanism of κ-carbide in austenite was found in 1986 by Bentley et al. [49], and Chu et al. [50] obtained similar results in 1992. Additionally, the formation mechanism of κ-carbide in austenite was also analyzed from a thermodynamic perspective by Yang et al. [51]. The orientation relationships between κ-carbide and austenite matrix are $(011)_\kappa//(001)_\gamma$ and $[001]_\kappa//[001]_\gamma$ (Figure 3c), and the lattice misfit along $[001]_\kappa//[001]_\gamma$ was calculated to be 2.70% [15]. The low lattice misfit signifies a small elastic strain energy, which induces the spinodal decomposition at low undercooling, and it was also able to

produce excellent mechanical properties [52,53]. Aging at 600 °C for less than 100 h, a cuboidal nano-sized κ-carbide has been observed in previous studies to precipitate in austenitic Fe-Mn-Al-C steels [54–57]. Bartlett et al. [53] investigated the effect of silicon on κ-carbide precipitation in austenite, and found that silicon accelerates the formation of κ-carbide, but does not increase its fraction. Their results also suggested that phosphorus increases the initial ordering reaction, and accelerates the spinodal decomposition for κ-carbide precipitation in the latter stage [58]. Moon et al. [48] found that molybdenum delays the precipitation of κ-carbide, owing to an increased strain energy between κ-carbide and austenite by molybdenum addition. The results of Sutou et al. [8] showed that chromium does not partition into κ-carbide and delays the precipitation of κ-carbide.

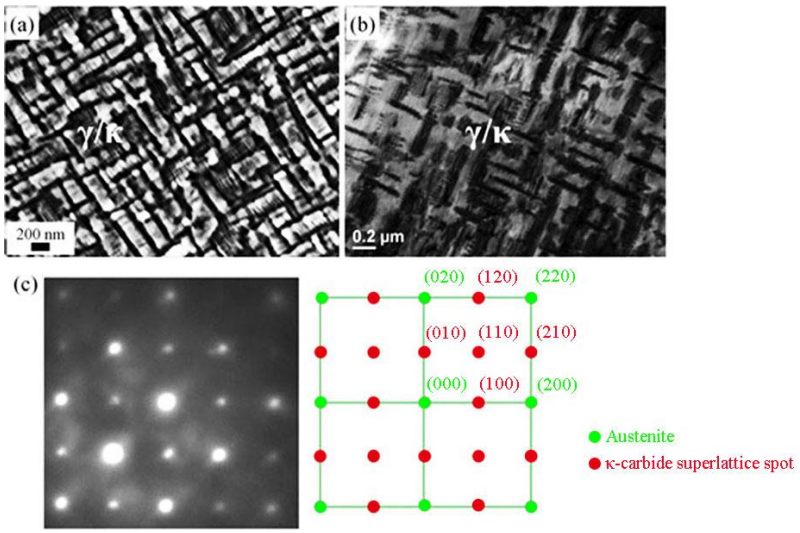

Figure 3. (**a**) SEM image of κ-carbide in austenite, (**b**) TEM bright field image of fine κ-carbide in austenite, and (**c**) TEM diffraction pattern from selected γ/κ area. (Reprinted with permission from [15], copyright Taylor and Francis, 2015).

3.3. Formation of κ-Carbide in Ferrite Matrix

The microstructures of κ-carbide formed in the ferrite-based low-density Fe-Mn-Al-C alloy are illustrated in Figure 4, and are formed by a typical eutectoid reaction of $\gamma \rightarrow \alpha + \kappa$ associated with nucleation and growth [15,59]. The orientation relationships between κ-carbide and ferrite are $(111)_\kappa // (110)_\alpha$ and $[011]_\kappa // [001]_\alpha$ (Figure 4a), corresponding to the well-known Nishiyama–Wasserman (N-W) relationship. The interface between κ-carbide and ferrite is semi-coherent, and verified by misfit dislocations ('D') (Figure 4b), and the lattice misfit is high, and was measured to be nearly 5.9% by Seol et al. [59], while it was calculated to be 6.67% along $[011]_\kappa // [001]_\alpha$ by Lu et al. [15], resulting in an elongated rod-type morphology of κ-carbide. Additionally, carbon and aluminum promote and stabilize the precipitation of κ-carbide [60,61]. The low solubility of carbon in ferrite also facilitates the stabilization of κ-carbide [15]. The nucleation/growth of κ-carbide is determined by the diffusion of carbon and aluminum. Jeong et al. [62] observed that austenite decomposed into ferrite and κ-carbide by means of a eutectoid reaction after aging at 550 °C for 5 h, and the κ-carbide was precipitated quickly at the boundaries after aging at 550 °C for 1 h, due to the pre-segregation of solute atoms at both the grain and interphase boundaries.

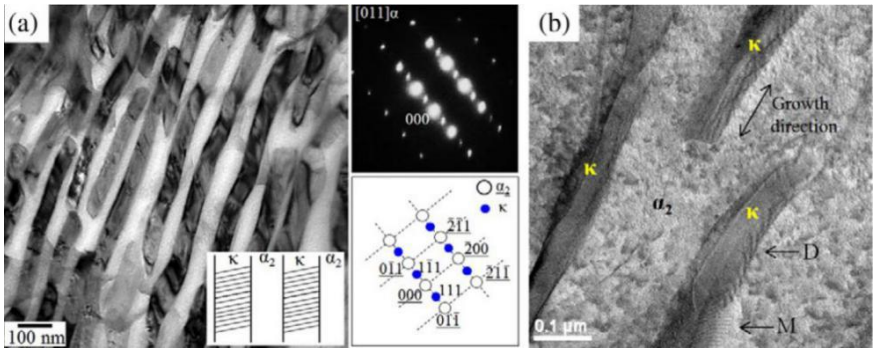

Figure 4. (**a**) TEM micrograph and the corresponding SADP of $[011]_\alpha$ zone for the steel isothermally annealed at 600 °C and (**b**) Cs-corrected (S) TEM bright-field image. D, dislocations. (Reprinted with permission from [59], copyright Elsevier, 2013).

4. Effect of κ-Carbide on Mechanical Properties

4.1. Austenite-Based Fe-Mn-Al-C Steels

Austenite-based Fe-Mn-Al-C steels, with compositions of 15–30 wt.% Mn, 5–7 wt.% Al and 0.5–1.2 wt.% C, offer a combination of outstanding mechanical properties, which have been widely investigated [3–5,10,63–65]. The addition of Al promotes the precipitation of κ-carbide and thus significantly affects the mechanical strength [2]. The precipitation of coarse κ-carbide or/and thick κ-carbide film on the austenite grain boundaries was found to be one of the reasons for the deterioration of ductility, as a result of the increased ease of stress concentration at boundaries [2,62]. Nano-sized κ-carbide precipitation is responsible for the high strength, hardness and good ductility of austenitic steels. Ding et al. [66] reported that the precipitation strengthening effect of nano-sized κ-carbide on the yield strength was about 1.78 times the size of the effect of strengthening from the Al solution (Figure 5). Sutou et al. [8] investigated austenitic steels with excellent ductility and high hardness and strength, which is also related to the precipitation of nano-sized κ-carbide. In their results, Fe-20Mn-11Al-1.8C-5Cr showed a hardness of 427 HV, a tensile strength of 1223 MPa, an elongation of 41%, and especially a higher specific strength than that of conventional steels [8]. Considering the influence of intergranular κ-carbide on fracture behavior and the beneficial effect of nano-sized intragranular κ-carbide on mechanical properties, the control of κ-carbide precipitation was achieved by varying the cooling pattern or alloy addition [8,19,48,58]. With the cooling path of Fe-11Mn-9Al-1.25C steels changing from air cooling to intensive quenching, intergranular κ-carbides with a size of 0.6–2.6 μm were inhibited, and intra-granular κ-carbides with sizes smaller than 13 nm were observed [19].

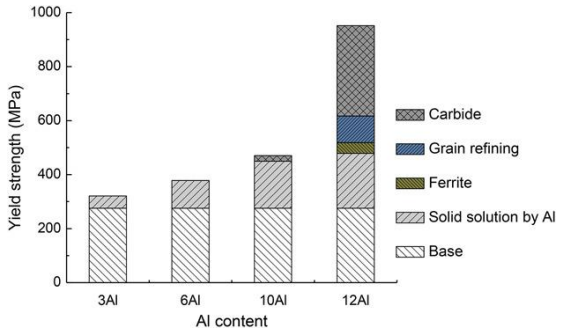

Figure 5. Diagram indicating the different mechanisms contributing to the yield strength of Fe-26Mn-xAl-1C steels. (Reprinted with permission from [66], copyright Wiley, 2017).

Investigations on the interaction mechanism of dislocation/κ-carbide are crucial for understanding how κ-carbide precipitation affects mechanical behavior. Frommeyer and Brüx [3] reported that a

regular distribution of nano-sized κ-carbide coherent with austenite sustained a shear band-induced plasticity (SIP) effect, namely, the formation of uniformly arranged shear bands on {111} planes accompanied by dislocation gliding, which formed the main contribution to ductility (Figure 6). Their results were different from those reported in some earlier studies, in which martensite transformation and/or twinning was regarded as the dominant deformation mechanism [63]. The SIP mechanism was also discussed by Choi et al. [55], Wu et al. [4] and Hasse et al. [64], who only focused on the shearing of κ-carbide. In contrast, Rabbe et al. [5] and Gutierre-Urrutia et al. [10] discussed a novel insight on dislocation/κ-carbide interaction. Their observations demonstrated that the predominant deformation mechanisms were the Orowan bypassing of rod-shaped κ-carbide, the cross-slip assisting the subsequent expansion of dislocation loops, and, to a lesser extent, the shearing of κ-carbide (Figure 7) [10]. The activation of Orowan bypassing and dislocations held at austenite/κ-carbide interfaces was observed, as shown in Figure 7b. The interaction mechanism related to the volume fraction and average radius of κ-carbide was then proposed by Kim et al. [65]. Their results indicated that the dominant deformation mechanism changes from shearing of smaller κ-carbide precipitation to bypassing of larger precipitation at a certain volume fraction, and the critical radius was evaluated to be 13.4 nm (Figure 8).

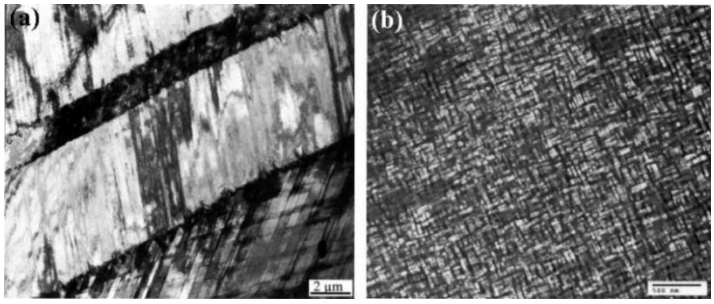

Figure 6. (**a**) TEM bright-field image exhibiting shear bands on {111} planes in the austenitic matrix, (**b**) TEM dark-field image showing the regular arrangement of κ-carbides. (Reprinted with permission from [3], copyright Wiley, 2016).

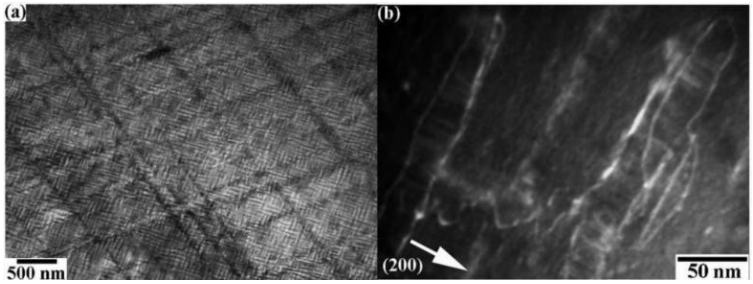

Figure 7. (**a**) TEM image of planar dislocation arrangements, (**b**) weak beam TEM images of dislocation/κ-carbides interactions in Fe-30.5Mn-8.0Al-1.2C (wt.%) steel aged at 600 °C for 24 h and tensile deformed to 0.15 true strain: diffraction vectors are indicated by arrows. (Reprinted with permission from [10], copyright Taylor and Francis, 2014).

Fe-30Mn-9Al-0.9C (wt.%) steel was experimentally examined and found to exhibit a Charpy V-notch (CVN) impact energy of up to 200 J at room temperature [67]. The notch toughness of solution-treated Fe-30Mn-9Al-0.9C-1Si (wt.%) steels decreased from 200 J to 28 J when increasing the phosphorus content from 0.001 wt.% to 0.07 wt.%, due to the promotion of κ-carbide precipitation along the grain boundaries. The increase in phosphorus content from 0.001 wt.% to 0.043 wt.% also reduced the dynamic fracture toughness from 376 kJ/m^2 to 100 kJ/m^2. The silicon content had a similar effect on the notch toughness and dynamic fracture toughness, resulting from the acceleration of κ-carbide formation at boundaries.

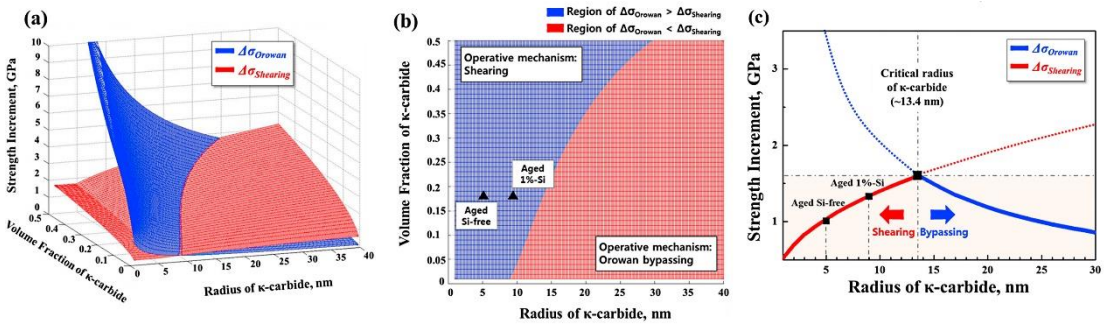

Figure 8. Relationship between operative deformation mechanism (as the lowest strength increment), volume fraction and average radius of κ-carbide is shown in (**a**). Top-view of (**a**) is present in (**b**). For a volume fraction of κ-carbide of 0.18, the curves of strength increment–radius are shown in (**c**), which indicates that the critical radius of κ-carbide is 13.4 nm. (Reprinted with permission from [65], copyright Elsevier, 2019).

4.2. Ferrite-Based Fe-Mn-Al-C Steels

Through a eutectoid reaction of austenite, the κ-carbide is able to present a lamellar structure with ferrite, known as κ-pearlite, which exhibits a similar structure to that of θ-pearlite (cementite+ferrite) [20,68]. Under the same mean inter-lamellar spacing, κ-pearlite exhibits a much higher yield strength and hardness compared with θ-pearlite [68]. For example, Fe-8Mn-13Al-7C (at.%) steel possesses a yield stress of 1880 MPa and a hardness of 580 HV, while the high-carbon θ-pearlite in GCr15 bearing steel possesses a hardness of only 367 HV [20,68]. Additionally, the mean inter-lamellar spacing of κ-pearlite is usually smaller than that of θ-pearlite, since the necessary aluminum diffusion decreases the kinetics of lamellar thickening [69]. Therefore, κ-pearlite is stronger than θ-pearlite, according to the Hall-Petch relationship [68,70]. However, κ-pearlite possesses poor ductility, which can mainly be attributed to the large fraction of carbide in κ-pearlite, resulting from the higher level of eutectoid carbon content by aluminum addition [71,72]. Therefore, subcritical spheroidization annealing was first proposed by Chen et al. to improve the ductility of κ-pearlite [20]. More specifically, after annealing at 700 °C for 32 h, the total elongation of Fe-0.55C-1Mn-5Al (wt.%) increased from 13% to 28%, and the fracture mode changed from brittle to ductile (Figure 9) [20].

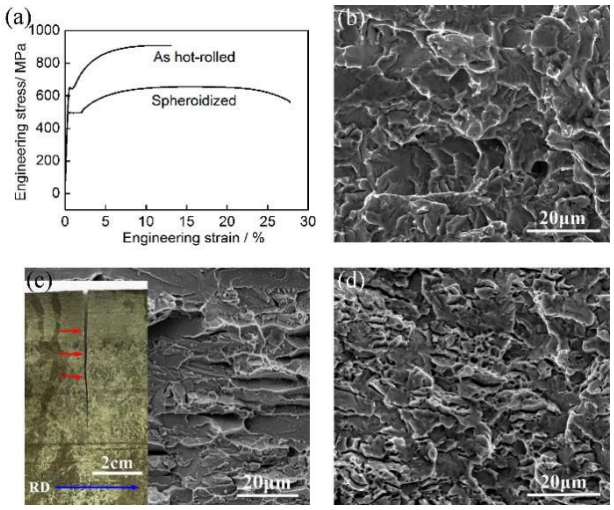

Figure 9. Tensile mechanical properties and SEM images of fracture morphology of the as hot-rolled and spheroidized steels. (**a**) Engineering stress–strain curves; (**b**) tensile fracture of the as hot-rolled steel showing quasi-cleavage fracture; (**c**) cold-rolling fracture of the as hot-rolled steel; (**d**) tensile fracture of spheroidized alloy exhibiting ductile fracture with some spherical dimples. (Reprinted with permission from [20], copyright Elsevier, 2016).

The intergranular κ-carbide is undesirable in ferrite-based alloys as well, as it works to initiate cracking or facilitate crack propagation. It was suggested by Shin et al. [73] that intergranular κ-carbide could be suppressed by increasing the finishing-rolling temperature to above 900 °C during hot-rolling, reducing central segregation during the slab-making process, or reducing material variation during hot-rolling. Han et al. [74] reported that increasing carbon content from 0.1 wt.% to 0.3 wt.% could effectively reduce the formation of interfacial κ-carbide, thus leading to a simultaneous enhancement of strength and ductility. Han et al. [75] also found that the appropriate annealing temperature and carbon content could achieve a fine κ-carbide distribution in ferrite-based steels, thereby bringing about an improvement in both strength and ductility.

4.3. Duplex-Phase Fe-Mn-Al-C Steels

The mechanical properties of duplex-phase Fe-Mn-Al-C steels are determined by the microstructures of austenite, ferrite and κ-carbide. As κ-carbide has different precipitation kinetics in austenite and ferrite, it is necessary to design a thermomechanical process to obtain a suitable microstructure in light-weight steels with satisfactory mechanical properties [15]. The hardness of duplex steels annealed at 700 °C was measured to be 704 ± 23 HV for austenite containing κ-carbide and 526 ± 20 HV for ferrite with κ-carbide [15]. Song et al. [76] studied the effect of κ-carbide on the tensile properties of duplex-phase Fe-Mn-Al-C steels, and they reported that the morphological change from lamellar to polygonal and the reduction in volume fraction of κ-carbide decreased the strength but increased the ductility. For instance, the overall tensile properties of duplex-phase steels with compositions of Fe-0.8C-12Mn-7Al (wt.%) were greatly improved by modifying the morphology and fraction of κ-carbide after a suitable annealing heat treatment [76]. Annealing at 800 °C increased the elongation of Fe-0.8C-12Mn-7A steels from 2.6% to 34.8% (Figure 10), and increasing manganese content from 12 wt.% to 15 wt.% or 20 wt.% could effectively decrease the fraction of lamellar κ-carbides at the grain boundaries, which has a negative effect on the mechanical properties.

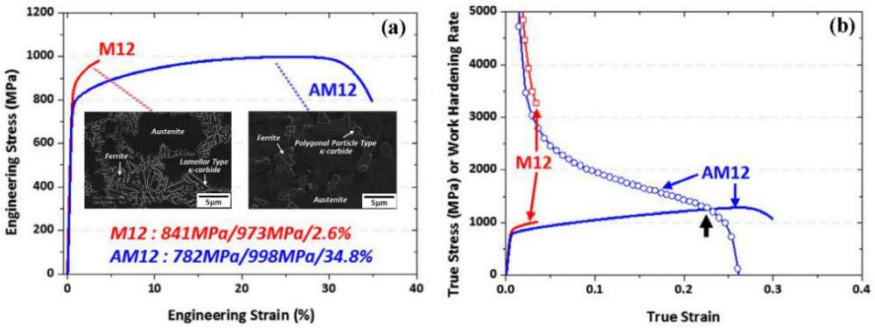

Figure 10. (**a**) Engineering stress–strain curves and microstructures, (**b**) true stress–strain curves and work hardening rate curves of hot-rolled alloy (M12) and annealing alloy (AM12) with the compositions of Fe-0.8C-12Mn-7Al (wt.%). (Adapted with permission from [76], copyright Elsevier, 2018).

5. Conclusions and Perspectives

κ-carbides are critical precipitates in Fe-Mn-Al-C steels, as they have a significant influence on the relevant properties. In this paper, the structures, formation mechanism and operative deformation mechanism of κ-carbide are reviewed, and the major relevant characteristics are summarized in Figure 11.

The κ-carbide is a carbide with an *L*'l-type structure that has a perfect formula of $(Fe,Mn)_3AlC$, while the lattice parameters vary with carbon and manganese content. The addition of manganese has a great effect on its elastic and magnetic properties. The equilibrium thermodynamic of κ-carbide precipitation facilitates the design of microstructures. Thus, the accuracy of the thermodynamic database of the Fe-Mn-Al-C system needs to be substantially improved to include a more accurate description of κ-carbide precipitation. The κ-carbide is precipitated in the austenite matrix in a typical

spinodal decomposition, which is mainly determined by fluctuations in the composition of aluminum and carbon, and there is no nucleation stage, while the κ-carbide is formed by a typical eutectoid reaction associated with nucleation and growth. A coherent interface is obtained between κ-carbide and austenite with a low lattice misfit, whereas the κ-carbide/ferrite interface is semi-coherent with a higher lattice misfit. Although different precipitation mechanisms have been found in austenite and ferrite matrices, further clarifications on the precipitation mechanisms of κ-carbide are still needed to obtain a more effective adjustment of microstructures.

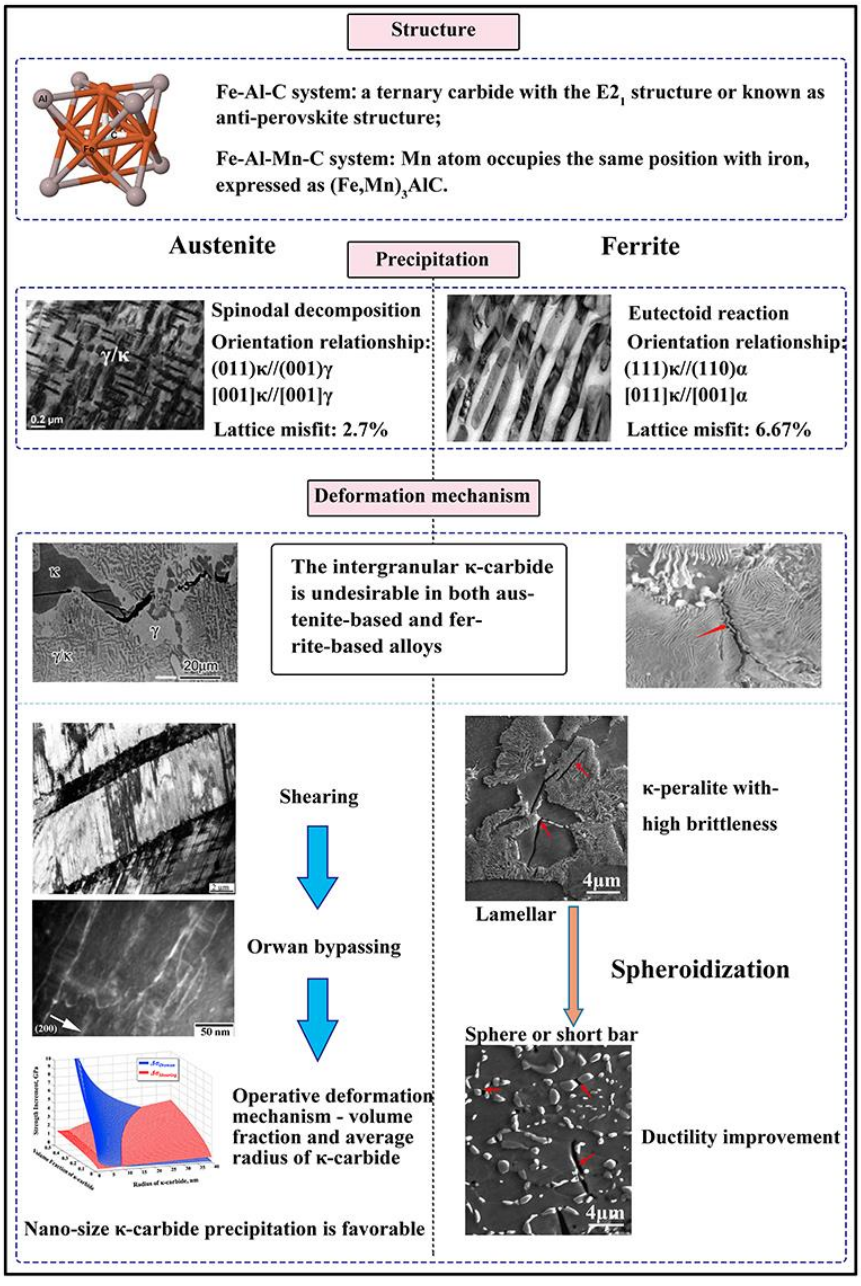

Figure 11. Overall view of the precipitation and deformation of κ-carbide in Fe-Mn-Al-C steels. (Adapted with permission from [2], copyright Elsevier, 2004; [3] Wiley, 2016; [10] Taylor and Francis, 2004; [15] Taylor and Francis, 2015; [21] Elsevier, 2008; [65] Elsevier, 2019 and [20] Elsevier, 2019).

The operative deformation mechanisms related to κ-carbide in Fe-Mn-Al-C steels were tentatively revealed. Nano-sized κ-carbide uniformly distributed in austenite is beneficial for the simultaneous enhancement of strength and ductility. The dominant deformation mechanism on κ-carbide particles in

austenite-based Fe-Mn-Al-C steels changes from shearing for large-sized particles to Orwan bypassing for smaller ones. The lamellar κ-pearlite (κ-carbide + ferrite) formed by a eutectoid reaction may cause a high brittleness. A spheroidization heat treatment could significantly improve the ductility of ferrite-based steels by reducing the stress concentration on the carbides. It is now recognized that κ-carbides on grain boundaries are unfavorable, and an appropriate control of the morphology, size and distribution of κ-carbide is necessary to obtain the desired mechanical properties. The effect of κ-carbides on plasticity and fracture mechanisms is still an important subject and needs to be further investigated.

Other properties, such as fatigue properties, and formability, weldability and coatability of Fe-Mn-Al-C steels are also of particular significance for their future industrialization. However, the available information about these properties is still rather limited, and a great deal of experimental effort is urgently needed in this respect to clarify the probably positive impact of κ-carbides on these properties.

Author Contributions: Writing—Original Draft Preparation and funding acquisition, P.C.; Writing—Review & Editing, X.L.; Writing—Review & Editing and funding acquisition, H.Y. All authors have read and agreed to the published version of the manuscript.

Funding: This research was funded by National Natural Science Foundation of China, grant numbers. 51804072 and 51722402; Fundamental Research Funds for the Central University, grant number N2007012; China Postdoctoral Science Foundation, grant number 2018M631802; 111 Project, grant number B16009 and Liaoning Revitalization Talents Program, grant number xlyc1907128.

Conflicts of Interest: The authors declare no conflict of interest.

References

1. Chen, S.; Rana, R.; Haldar, A.; Ray, R.K. Current state of Fe-Mn-Al-C low density steels. *Prog. Mater. Sci.* **2017**, *89*, 345–391. [CrossRef]
2. Kimura, Y.; Handa, K.; Hayashi, K.; Mishima, Y. Microstructure control and ductility improvement of the two-phase γ-Fe/κ-(Fe, Mn)3AlC alloys in the Fe–Mn–Al–C quaternary system. *Intermetallics* **2004**, *12*, 607–617. [CrossRef]
3. Frommeyer, G.; Brüx, U. Microstructures and Mechanical Properties of High-Strength Fe-Mn-Al-C Light-Weight TRIPLEX Steels. *Steel Res. Int.* **2006**, *77*, 627–633. [CrossRef]
4. Wu, Z.Q.; Ding, H.; Li, H.Y.; Huang, M.L.; Cao, F.R. Microstructural evolution and strain hardening behavior during plastic deformation of Fe–12Mn–8Al–0.8C steel. *Mater. Sci. Eng. A* **2013**, *584*, 150–155. [CrossRef]
5. Raabe, D.; Springer, H.; Gutierrez-Urrutia, I.; Roters, F.; Bausch, M.; Seol, J.B.; Koyama, M.; Choi, P.P.; Tsuzaki, K. Alloy Design, Combinatorial Synthesis, and Microstructure–Property Relations for Low-Density Fe-Mn-Al-C Austenitic Steels. *JOM* **2014**, *66*, 1845–1856. [CrossRef]
6. Kalashnikov, I.; Shalkevich, A.; Acselrad, O.; Pereira, L.C. Chemical composition optimization for austenitic steels of the Fe-Mn-Al-C system. *J. Mater. Eng. Perform.* **2000**, *9*, 597–602. [CrossRef]
7. Howell, R.A.; Aken, D.C. A literature review of age hardening Fe-Mn-Al-C alloys. *Iron Steel Technol.* **2009**, *6*, 193–212.
8. Sutou, Y.; Kamiya, N.; Umino, R.; Ohnuma, I.; Ishida, K. High-strength Fe–20Mn–Al–C-based Alloys with Low Density. *ISIJ Int.* **2010**, *50*, 893–899. [CrossRef]
9. Kim, H.; Suh, D.-W.; Kim, N.J. Fe–Al–Mn–C lightweight structural alloys: A review on the microstructures and mechanical properties. *Sci. Technol. Adv. Mater.* **2013**, *14*, 014205. [CrossRef]
10. Gutierrez-Urrutia, I.; Raabe, D. High strength and ductile low density austenitic FeMnAlC steels: Simplex and alloys strengthened by nanoscale ordered carbides. *Mater. Sci. Technol.* **2014**, *30*, 1099–1104. [CrossRef]
11. Ding, H.; Han, D.; Zhang, J.; Cai, Z.; Wu, Z.; Cai, M. Tensile deformation behavior analysis of low density Fe–18Mn–10Al–xC steels. *Mater. Sci. Eng. A* **2016**, *652*, 69–76. [CrossRef]
12. Frommeyer, G.; Drewes, E.J.; Engl, B. Physical and mechanical properties of iron-aluminium-(Mn, Si) lightweight steels. *Rev. De Metall. Cah. D Inf. Tech.* **2000**, *97*, 1245–1253. [CrossRef]
13. Chin, K.; Lee, H.; Kwak, J.; Kang, J.; Lee, B. Thermodynamic calculation on the stability of (Fe,Mn)3AlC carbide in high aluminum steels. *J. Alloy. Compd.* **2010**, *505*, 217–223. [CrossRef]

14. Jiménez, J.A.; Frommeyer, G. The ternary iron aluminum carbides. *J. Alloy. Compd.* **2011**, *509*, 2729–2733. [CrossRef]
15. Lu, W.J.; Zhang, X.F.; Qin, R.S. Structure and properties of κ-carbides in duplex lightweight steels. *Ironmak. Steelmak.* **2015**, *42*, 626–631. [CrossRef]
16. Grässel, O.; Frommeyer, G. Effect of martensitic phase transformation and deformation twinning on mechanical properties of Fe–Mn–Si–AI steels. *Mater. Sci. Technol.* **1998**, *14*, 1213–1217. [CrossRef]
17. Frommeyer, G.; Jiménez, J.A. Structural superplasticity at higher strain rates of hypereutectoid Fe-5.5Al-1Sn-1Cr-1.3C steel. *Metall. Mater. Trans. A* **2005**, *36*, 295–300. [CrossRef]
18. Kim, K.-H.; Lee, J.-S.; Lee, D.-L. Effect of silicon on the spheroidization of cementite in hypereutectoid high carbon chromium bearing steels. *Met. Mater. Int.* **2010**, *16*, 871–876. [CrossRef]
19. Liu, D.; Cai, M.; Ding, H.; Han, D. Control of inter/intra-granular κ-carbides and its influence on overall mechanical properties of a Fe-11Mn-10Al-1.25C low density steel. *Mater. Sci. Eng. A* **2018**, *715*, 25–32. [CrossRef]
20. Chen, P.; Xiong, X.C.; Wang, G.D.; Yi, H.L. The origin of the brittleness of high aluminum pearlite and the method for improving ductility. *Scr. Mater.* **2016**, *124*, 42–46. [CrossRef]
21. Connetable, D.; Maugis, P. First principle calculations of the κ-Fe3AlC perovskite and iron–aluminium intermetallics. *Intermetallics* **2008**, *16*, 345–352. [CrossRef]
22. Noh, J.Y.; Kim, H. Ab initiocalculations on the effect of Mn substitution in theκ-carbide Fe3AlC. *J. Korean Phys. Soc.* **2013**, *62*, 481–485. [CrossRef]
23. Palm, M.; Inden, G. Experimental determination of phase equilibria in the Fe-Al-C system. *Intermetallics* **1995**, *3*, 443–454. [CrossRef]
24. Andryushchenko, V.A.; Gavrilyuk, V.G.; Nadutov, V.M. Atomic and magnetic ordering in the κ-phase of Fe-Al-C alloys. *Phys. Met. Metallogr.* **1985**, *60*, 50–55.
25. Yang, J.; La, P.; Liu, W.; Hao, Y. Microstructure and properties of Fe3Al–Fe3AlC0.5 composites prepared by self-propagating high temperature synthesis casting. *Mater. Sci. Eng. A* **2004**, *382*, 8–14. [CrossRef]
26. Huetter, L.J.; Stadelmaier, H.H. Ternary carbides of transition metals with aluminum and magnesium. *Acta Metall.* **1958**, *6*, 367–370. [CrossRef]
27. Choo, W.K.; Han, K.H. Phase constitution and lattice parameter relationships in rapidly solidified (Fe0.65Mn0.35)0.83 Al0.17-xC and Fe3Al-xC pseudo-binary alloys. *Metall. Mater. Trans. A* **1985**, *16*, 5–10. [CrossRef]
28. Hosoda, H.; Miyazaki, S.; Mishima, Y. Phase constitution of some intermetallics in continuous quaternary pillar phase diagrams. *J. Phase Equilibria* **2001**, *22*, 394–399. [CrossRef]
29. Dierkes, H.; Leusen, J.V.; Bogdanovski, D.; Dronskowski, R. Synthesis, Crystal Structure, Magnetic Properties, and Stability of the Manganese-Rich "Mn3AlC" κ Phase. *Inorg. Chem.* **2017**, *56*, 1045–1048. [CrossRef]
30. Kellou, A.; Grosdidier, T.; Raulot, J.M.; Aourag, H. Atomistic study of magnetism effect on structural stability in Fe3Al and Fe3AlX (X = H, B, C, N, O) alloys. *Phys. Status Solidi* **2008**, *245*, 750–755. [CrossRef]
31. Briggs, I.; Russell, G.J.; Clegg, A.G. Some structural and magnetic properties of Fe-Al-C and Fe-Mn-Al-C alloys. *J. Mater. Sci.* **1985**, *20*, 668–673. [CrossRef]
32. Jiyoung, N.; Hanchul, K. Density Functional Theory Calculations on kappa-carbides, (Fe,Mn)3AlC. *J. Korean Phys. Soc.* **2011**, *58*, 285–290.
33. Meyer, L.; Bühler, H.E. Aufbau von Diffusionsschichten zwischen unlegiertem Stahl und Aluminium (Construction of diffusion-layers of unalloyed steel and aluminium). *Aluminium* **1967**, *43*, 733–738.
34. Parker, S.F.H.; Grundy, P.J.; Jones, G.A.; Briggs, I.; Clegg, A.G. Microstructure and magnetic properties of the permanent magnet material FeAIC. *J. Mater. Sci.* **1988**, *23*, 217–222. [CrossRef]
35. Reddy, B.V.; Khanna, S.N. Chemically induced oscillatory exchange coupling in chromium oxide clusters. *Phys. Rev. Lett.* **1999**, *83*, 3170–3173. [CrossRef]
36. Reddy, B.V.; Deevi, S.C. Local interactions of carbon in FeAl alloys. *Mater. Sci. Eng. A* **2002**, *329*, 395–401. [CrossRef]
37. Cheng, W. Formation of a New Phase after High-Temperature Annealing and Air Cooling of an Fe-Mn-Al Alloy. *Metall. Mater. Trans. A* **2005**, *36*, 1737–1743. [CrossRef]
38. Cheng, W.; Song, Y.; Lin, Y.; Chen, K.; Pistorius, P.C. On the Eutectoid Reaction in a Quaternary Fe-C-Mn-Al Alloy: Austenite → Ferrite + Kappa-Carbide + M23C6 Carbide. *Metall. Mater. Trans. A* **2014**, *45*, 1199–1216. [CrossRef]

39. Kim, M.-S.; Kang, Y.-B. Development of thermodynamic database for high Mn–high Al steels: Phase equilibria in the Fe–Mn–Al–C system by experiment and thermodynamic modeling. *Calphad* **2015**, *51*, 89–103. [CrossRef]
40. Connetable, D.; Lacaze, J.; Maugis, P.; Sundman, B. A Calphad assessment of Al–C–Fe system with the κ carbide modelled as an ordered form of the fcc phase. *Calphad* **2008**, *32*, 361–370. [CrossRef]
41. Ishida, K.; Ohtani, H.; Satoh, N.; Kainuma, R.; Nishizawa, T. Phase Equilibria in Fe-Mn-Al-C Alloys. *ISIJ Int.* **1990**, *30*, 680–686. [CrossRef]
42. Kim, M.-S.; Kang, Y.-B. Thermodynamic Modeling of the Fe-Mn-C and the Fe-Mn-Al Systems Using the Modified Quasichemical Model for Liquid Phase. *J. Phase Equilibria Diffus.* **2015**, *36*, 453–470. [CrossRef]
43. Kumar, K.C.H.; Raghavan, V. A Thermodynamic Analysis of the Al-C-Fe System. *J. Phase Equilibria* **1991**, *12*, 275–286. [CrossRef]
44. Raghavan, V. Al-C-Fe (aluminum-carbon-iron). *Cheminform* **1993**, *34*, 615–617.
45. Raghavan, V. Al-C-Fe (Aluminum-Carbon-Iron). *J. Phase Equilibria* **2002**, *23*, 508–510. [CrossRef]
46. Raghavan, V. Al-C-Fe (Aluminiun-Carbon-Iron). *J. Phase Equilibria Diffus.* **2007**, *28*, 267–268. [CrossRef]
47. Phan, A.T.; Paek, M.K.; Kang, Y.B. Phase equilibria and thermodynamics of the Fe–Al–C system: Critical evaluation, experiment and thermodynamic optimization. *Acta Materialia* **2014**, *79*, 1–15. [CrossRef]
48. Moon, J.; Park, S.; Jang, J.H.; Lee, T.; Lee, C.; Hong, H.; Suh, D.; Kim, S.; Han, H.N.; Lee, B.H. Atomistic investigations of κ-carbide precipitation in austenitic Fe-Mn-Al-C lightweight steels and the effect of Mo addition. *Scr. Mater.* **2017**, *127*, 97–101. [CrossRef]
49. Bentley, A.P. Ordering in Fe-Mn-Al-C austenite. *J. Mater. Sci. Lett.* **1986**, *5*, 907–908. [CrossRef]
50. Chu, S.M.; Kao, P.W.; Gan, D. Growth kinetics of κ-carbide particles in Fe-30Mn-10Al-1C-1Si alloy. *Scr. Metall. Et Mater.* **1992**, *26*, 1067–1070. [CrossRef]
51. Yang, L.; Huang, F.; Guo, Z.; Rong, Y.; Chen, N. Investigation on the formation mechanism of ordered carbide (FeMn)3AlC in the Al added twinning-induced plasticity steels. *J. Shanghai Jiaotong Univ.* **2016**, *21*, 406–410. [CrossRef]
52. Lu, K.; Lu, L.; Suresh, S. Strengthening Materials by Engineering Coherent Internal Boundaries at the Nanoscale. *Science* **2009**, *324*, 349–352. [CrossRef] [PubMed]
53. Bartlett, L.N.; Van Aken, D.C.; Medvedeva, J.; Isheim, D.; Medvedeva, N.; Song, K. An Atom Probe Study of κ-carbide Precipitation in Austenitic Lightweight Steel and the Effect of Phosphorus. *Metall. Mater. Trans. A* **2017**, *48*, 5500–5515. [CrossRef]
54. Chang, K.M.; Chao, C.G.; Liu, T.F. Excellent combination of strength and ductility in an Fe–9Al–28Mn–1.8C alloy. *Scr. Mater.* **2010**, *63*, 162–165. [CrossRef]
55. Choi, K.; Seo, C.-H.; Lee, H.; Kim, S.K.; Kwak, J.H.; Chin, K.G.; Park, K.-T.; Kim, N.J. Effect of aging on the microstructure and deformation behavior of austenite base lightweight Fe–28Mn–9Al–0.8C steel. *Scr. Mater.* **2010**, *63*, 1028–1031. [CrossRef]
56. Chao, C.Y.; Hwang, C.N.; Liu, T.F. Grain boundary precipitation in an Fe-7.8Al-31.7Mn-0.54C alloy. *Scr. Metall. Et Mater.* **1993**, *28*, 109–114. [CrossRef]
57. Hwang, C.N.; Chao, C.Y.; Liu, T.F. Grain boundary precipitation in an Fe-8.0Al-31.5Mn-1.05C alloy. *Scr. Metall. Et Mater.* **1993**, *28*, 263–268. [CrossRef]
58. Bartlett, L.N. On the Effect of Silicon and Phosphorus During the Precipitation of Kappa-Carbide in Fe-Mn-Al-C Alloys. Ph.D. Thesis, Missouri University of Science and Technology, Rolla, MO, USA, 2013.
59. Seol, J.-B.; Raabe, D.; Choi, P.; Park, H.-S.; Kwak, J.H.; Park, C.-G. Direct evidence for the formation of ordered carbides in a ferrite-based low-density Fe–Mn–Al–C alloy studied by transmission electron microscopy and atom probe tomography. *Scr. Mater.* **2013**, *68*, 348–353. [CrossRef]
60. Heo, Y.-U.; Song, Y.-Y.; Park, S.-J.; Bhadeshia, H.K.D.H.; Suh, D.-W. Influence of Silicon in Low Density Fe-C-Mn-Al Steel. *Metall. Mater. Trans. A* **2012**, *43*, 1731–1735. [CrossRef]
61. Sato, K.; Tagawa, K.; Inoue, Y. Modulated structure and magnetic properties of age-hardenable Fe-Mn-Al-C alloys. *Metall. Trans. A* **1990**, *21*, 5–11. [CrossRef]
62. Jeong, J.; Lee, C.-Y.; Park, I.-J.; Lee, Y.-K. Isothermal precipitation behavior of κ-carbide in the Fe–9Mn–6Al–0.15C lightweight steel with a multiphase microstructure. *J. Alloy. Compd.* **2013**, *574*, 299–304. [CrossRef]
63. Sato, K.; Ichinose, M.; Hirotsu, Y.; Inoue, Y. Effects of deformation induced phase transformation and twinning on the mechanical properties of austenitic Fe-Mn-Al alloys. *ISIJ Int.* **1989**, *29*, 868–877. [CrossRef]

64. Haase, C.; Zehnder, C.; Ingendahl, T.; Bikar, A.; Tang, F.; Hallstedt, B.; Hu, W.; Bleck, W.; Molodov, D.A. On the deformation behavior of κ-carbide-free and κ-carbide-containing high-Mn light-weight steel. *Acta Mater.* **2017**, *122*, 332–343. [CrossRef]
65. Kim, C.W.; Terner, M.; Lee, J.H.; Hong, H.U.; Moon, J.; Park, S.J.; Jang, J.H.; Lee, C.H.; Lee, B.H.; Lee, Y.J. Partitioning of C into κ-carbides by Si addition and its effect on the initial deformation mechanism of Fe-Mn-Al-C lightweight steels. *J. Alloy. Compd.* **2019**, *775*, 554–564. [CrossRef]
66. Ding, H.; Li, H.; Misra, R.D.K.; Wu, Z.; Cai, M. Strengthening Mechanisms in Low Density Fe–26Mn–xAl–1C Steels. *Steel Res. Int.* **2018**, *89*, 1700381. [CrossRef]
67. Bartlett, L.; Van Aken, D. High Manganese and Aluminum Steels for the Military and Transportation Industry. *JOM* **2014**, *66*, 1770–1784. [CrossRef]
68. Ishii, H.; Ohkubo, K.; Miura, S.; Mohri, T. Mechanical Properties of α+κ Two-phase Lamellar Structure in Fe-Mn-Al-C Alloy. *Mater. Trans.* **2003**, *44*, 1679–1681. [CrossRef]
69. Yi, H.L.; Hou, Z.Y.; Xu, Y.B.; Wu, D.; Wang, G.D. Acceleration of spheroidization in eutectoid steels by the addition of aluminum. *Scr. Mater.* **2012**, *67*, 645–648. [CrossRef]
70. Embury, J.D.; Fisher, R.M. The structure and properties of drawn pearlite. *Acta Metall.* **1966**, *14*, 147–159. [CrossRef]
71. Yi, H.L.; Chen, P.; Hou, Z.Y.; Hong, N.; Cai, H.L.; Xu, Y.B.; Wu, D.; Wang, G.D. A novel design: Partitioning achieved by quenching and tempering (Q–T & P) in an aluminium-added low-density steel. *Scr. Mater.* **2013**, *68*, 370–374.
72. Chen, P.; Wang, G.D.; Xiong, X.C.; Yi, H.L. Abnormal expansion due to pearlite-to-austenite transformation in high aluminium-added steels. *Mater. Sci. Technol.* **2016**, *32*, 1678–1682. [CrossRef]
73. Shin, S.Y.; Lee, H.; Han, S.Y.; Seo, C.-H.; Choi, K.; Lee, S.; Kim, N.J.; Kwak, J.-H.; Chin, K.-G. Correlation of Microstructure and Cracking Phenomenon Occurring during Hot Rolling of Lightweight Steel Plates. *Metall. Mater. Trans. A* **2009**, *41*, 138–148. [CrossRef]
74. Han, S.Y.; Shin, S.Y.; Lee, S.; Kim, N.J.; Kwak, J.-H.; Chin, K.-G. Effect of Carbon Content on Cracking Phenomenon Occurring during Cold Rolling of Three Light-Weight Steel Plates. *Metall. Mater. Trans. A* **2010**, *42*, 138–146. [CrossRef]
75. Han, S.Y.; Shin, S.Y.; Lee, H.-J.; Lee, B.-J.; Lee, S.; Kim, N.J.; Kwak, J.-H. Effects of Annealing Temperature on Microstructure and Tensile Properties in Ferritic Lightweight Steels. *Metall. Mater. Trans. A* **2011**, *43*, 843–853. [CrossRef]
76. Song, H.; Kwon, Y.; Sohn, S.S.; Koo, M.; Kim, N.J.; Lee, B.-J.; Lee, S. Improvement of tensile properties in (austenite+ferrite+κ-carbide) triplex hot-rolled lightweight steels. *Mater. Sci. Eng. A* **2018**, *730*, 177–186. [CrossRef]